Electronic Supplementary Material (ESI) for CrystEngComm.
This journal is © The Royal Society of Chemistry 2016

Electronic Supplementary Information

Formation of Reworkable Nanocomposite Adhesives by Dielectric Heating of Epoxy Resin Embedded Fe_3O_4 Hollow Spheres

*Bin Zhao [a], Mark Hardiman [a], Kevin M. Ryan [b], Emmet O'Reilly [b], Conor McCarthy [a,] **

Irish Centre for Composites Research, Materials and Surface Science Institute, University of Limerick, Limerick, Ireland.

[a] Department of Mechanical, Aeronautical and Biomedical Engineering.

[b] Department of Chemical and Environmental Sciences.

* Corresponding author. E-mail address: Conor.McCarthy@ul.ie. Tel.: +353 61 234334; Fax: +353 61 202944.

Experimental Section

Synthesis of Fe_3O_4 hollow nanospheres

Based on the investigation on previous synthesis approaches about ZnO, TiO_2 and SiO_2 hollow nanospheres [1-4] as references, a mild alkaline reaction condition (e.g. ammonia, urea or HMTA, etc.) with the participation of surfactant (especially the cationic surfactant like CTAB) as the template is strongly of benefit for the formation of hollow spherical morphology. So the combination of HMTA and CTAB was selected as the typical synthesis procedure in this work.

0.006 mol CTAB and 0.0214 mol HMTA were dissolved in 60 mL ethylene glycol (EG), then 0.016 mol $FeCl_3 \cdot 6H_2O$ was added under continuous stirring until it was dissolved totally. The solution was transferred to a 100 ml Teflon-lined autoclave, then sealed and maintained at 220 ^oC for 12 h. After the autoclave cooled down to room temperature naturally, the black precipitate was washed with deionized water and absolute ethanol for several times and separated by magnetic decantation. Finally, the product was dried at 80 ^oC for 12 h under vacuum.

Characterizations for Fe_3O_4 HNSs

The size and morphology of Fe_3O_4 samples were characterized using field emission scanning electron microscopy (FESEM, Hitachi SU-70 system) at accelerating voltages of 10-20 kV. Specifically, powders of samples were mounted onto conductive copper tapes, which were then attached onto the surfaces of SEM brass stubs. The samples were then conductively coated with gold by a sputtering method to minimize charging effects under FESEM imaging conditions.

Both transmission electron microscopy (TEM) and high resolution transmission electron microscopy (HRTEM) characterizations were performed using a JEOL JEM 2100F field emission microscope equipped with a Gatan Ultrascan CCD camera and EDAX Genesis EDS facility, as well as with the potential of performing SAED. To prepare the HRTEM specimens, the powder samples were dispersed ultrasonically in anhydrous ethanol. One drop of the suspension was placed on a carbon film supported on a copper grid and allowed to dry in air before the specimens were transferred into the microscope.

X-ray diffraction (XRD) analysis was conducted using a PANalytical X'Pert PRO MRD instrument with a Cu K_α radiation source (λ = 1.5418 Å) and an X'celerator detector. Rietveld refinement was carried out using X'Pert High Score plus software.

Embedding Fe_3O_4 HNSs into epoxy resin to obtain the nanocomposite adhesive

In order to further verify the possibility of actual application, as well as the degradation performance of Fe_3O_4 HNSs in cured epoxy resin by dielectric heating, hardeners (MNA and DDSA, purchased from Sigma-Aldrich) and accelerator (DMP, purchased from Sigma-Aldrich) were added into the epoxy resin with Fe_3O_4 HNSs dispersed in it with stirring and sonication treatment in order to obtain a uniform dispersion. The uniform dispersion was then dropped onto a quartz slides, and transferred in vacuum oven at 60 ^oC for 3 days. Then the cured nanocomposite adhesive composite sheet (25.4 mm × 25.4 mm ×1 mm) was obtained for the further microwave degradation tests. For comparison, the pure epoxy resin sheet with the same size was also prepared and suffered the microwave irradiation in the same procedure.

Degradation procedure by dielectric heating

The as prepared nanocomposite adhesive (or cured pure epoxy resin) were placed into the focused microwave cavity of single mode microwave reactor (CEM, DISCOVER SP) with an infrared (IR) Temperature Sensor, as shown in Scheme 1a. The samples were exposed under single-mode microwave irradiation at fixed power of 100w and frequency at 2.45 GHz. The maximum irradiation time is 200 s and the safety temperature is 300 ^oC. The data with regard to the temperature as a function of time was collected by the compatible software "Synergy" provided by CEM Corporation installed in PC, which was connected to the single mode microwave reactor.

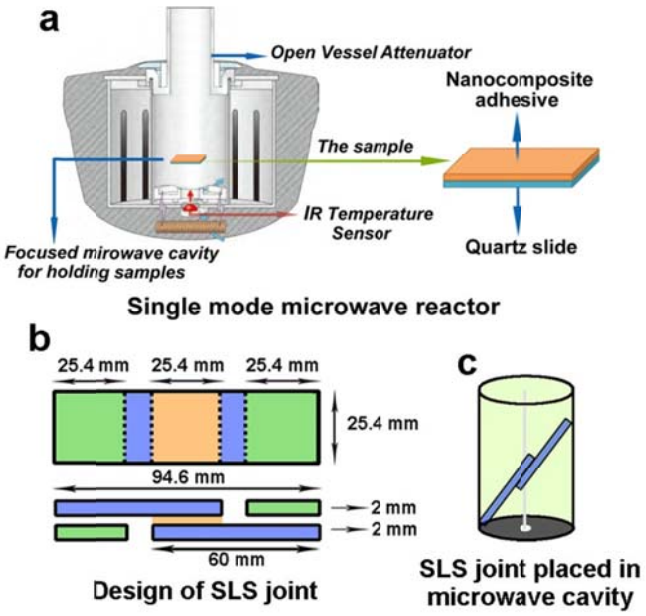

Scheme 1 Schematic illustrations of (a) the heating procedure of cured composites (1.0 wt% Fe_3O_4 HNSs in epoxy resin) in single mode microwave reactor CEM Discover SP; (b) geometrical parameters of the SLS joint; (c) the adhesively bonded SLS joint placed in the cavity of microwave reactor for further dielectric heating investigation.

Characterizations for nanocomposite adhesive

The cured Fe_3O_4-ER nanocomposite adhesive (or pure epoxy resin), obtained before and after microwave irradiation, were cut into small pieces (3mm×3mm×1mm) to expose the inner cross sections. Then these cross sections were attached onto the 90° chamfer of SEM stub for FESEM characterization. The samples were then conductively coated with gold by a sputtering method to minimize charging effects under FESEM imaging conditions.

The 3D internal morphologies of the cured Fe_3O_4-ER nanocomposite adhesive before and after 3mins' microwave irradiation were characterised by the non-destructive 3D X-ray microscopes (XRM), VersaXRM-500, employing at high-energy X-ray source (80kV) with optimised scintillators, multiple objective lenses and phase contrast imaging capabilities.

The hardness and modulus of the cured Fe_3O_4-ER composites (or pure epoxy resin), obtained before and after microwave irradiation, were characterised by nanoindentation. The procedures refer to the previous works in our group. [5] Before test, small sample pieces were mounted in clear epoxy cylinders with the fibre direction perpendicular to the top face of the cylinder in order to expose the cross sections. Mounting the samples in this way facilitated semi-automatic grinding and polishing down to a final polishing suspension particle size of 0.05 lm. The procedures used throughout the grinding and polishing sample preparation procedures were chosen to ensure that surface damage and reaction with the polishing agents were kept to a minimum. High depth CSM indentations were used to ensure there was no property change between that of the surface material and the material further from the surface as a result of the sample preparation procedures.

The nanoindentation experiments were carried out using the Nanoindenter G200 developed by Agilent Technologies. The continuous stiffness measurement (CSM) technique was used to carry out the indentations, which allowed the contact stiffness to be calculated throughout the indentation's loading cycle. This in turn allowed the elastic modulus to be calculated continuously as a function of the indentation depth, using the Oliver and Pharr method. [5] The load and displacement resolutions of the system are 50 nN and 0.01 nm respectively, and a Berkovich tip geometry was used. The indentations were assigned a maximum penetration depth setpoint of 5 μm with a strain rate target of 0.05/s. This strain rate target was reached with a maximum deviation of ±0.01/s for all depths deeper than 100 nm. The CSM settings were programmed to apply a harmonic displacement of 2 nm and a frequency of 45 Hz. The indentation sites were targeted using an optical microscope.

Tensile shear test

Fe_3O_4-ER nanocomposite adhesive (or pure epoxy resin as comparison) were used for bonding single-lap-shear (SLS) joints in this study. The configuration of the specimen is shown in Scheme 1b. The substrates are high stable epoxy plastic slides (60 mm x 25.4 mm x 2 mm) with no surface coating. 0.63 ml of uncured Fe_3O_4-ER nanocomposite adhesive (or pure epoxy resin) was used for bonding the joints with area of 25.4 mm x 25.4 mm. The total length of the bonded joints is 94.6 mm. Such customised dimension of SLS specimens is designed for matching the cavity size of microwave reactor in order to further investigate the degradation behaviour by dielectric heating (Scheme 1c, Fig. S1). Then the cured joints were exposed under single-mode microwave irradiation at fixed power of 100w and frequency at 2.45 GHz for 0-3 min.

A universal tensile machine (UTM, Tinius Olsen H25KS) was used to carry out the tensile shear tests [6, 7] at room temperature. In order to ensure that the loading direction was parallel to the bond-line, two compensation spacers (Fig. S1) were bonded with the SLS specimens after microwave irradiation. The crosshead velocity was set at a constant velocity of 2 mm/min. A minimum of three specimens for each surface condition was tested to produce at least 3 valid results. Then the intermediate data from 3 valid results, which was closest to the average value, was adopted to draw the load-displacement curve and calculate tensile shear strength.

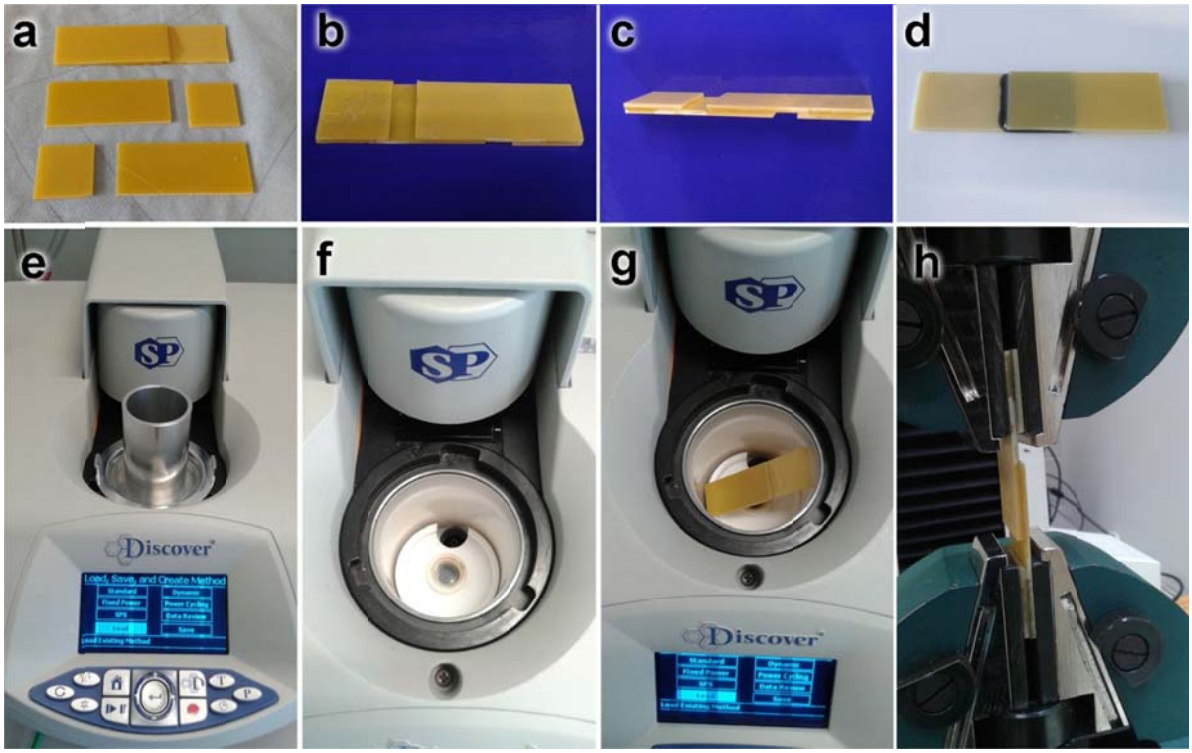

Fig. S1 (a-d) The geometrical design of the single lap-shear (SLS) joints and the joints adhesively bonded by the pure epoxy resin or Fe_3O_4-ER nanocomposite adhesive; (e-g) Such customised dimension of SLS specimens is designed for matching the cavity size of microwave reactor in order to further investigate the degradation behaviour by dielectric heating; (h) Tensile shear tests of single lap-shear (SLS) joints using the universal tensile machine (UTM, Tinius Olsen H25KS).

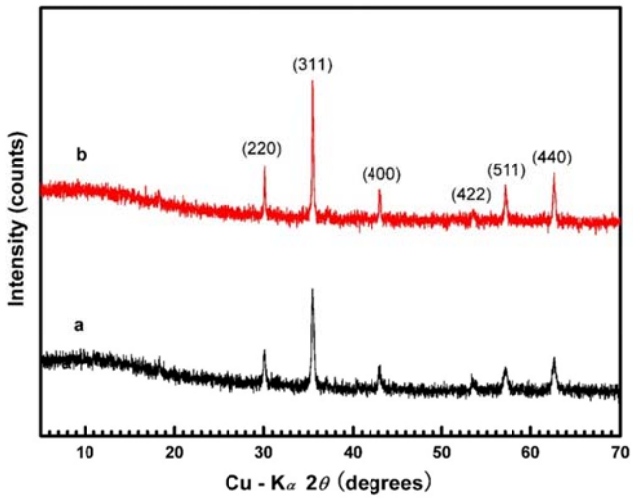

Fig. S2 XRD patterns of the products obtained in the typical procedure (a) and commercial Fe_3O_4 nanoparticles (b).

XRD pattern in Fig. S2a confirms the product obtained in the typical procedure is Fe_3O_4 polymorph, in which the diffraction peaks at at $2\theta \approx 30.1^{\circ}$, 35.4°, 43.1°, 56.9° and 62.5° correspond well with the (220), (311), (400), (511) and (440) lattice planes of magnetite Fe_3O_4 (JCPDS 19-0629) without any other impurity, which corresponds well with that of commercial Fe_3O_4 nanoparticles (Sigma-Aldrich, 50-100 nm) shown in Fig. S2b.

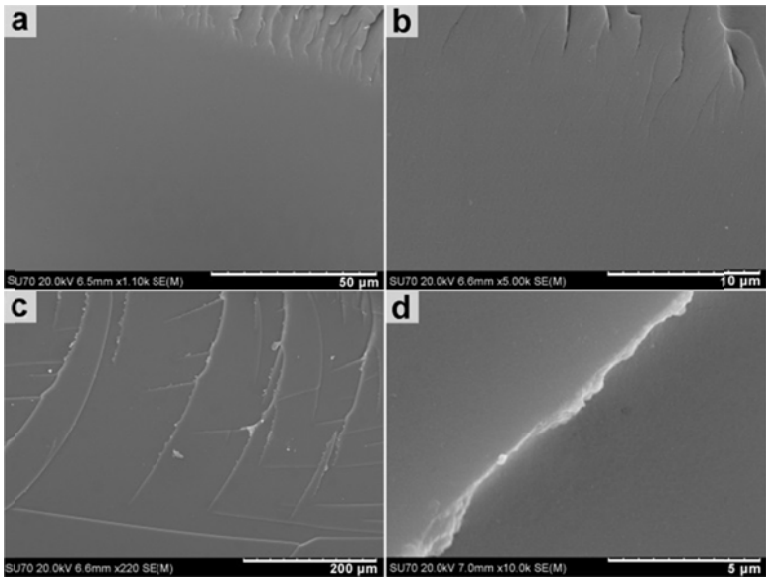

Fig. S3 FESEM images of the section facture of cured pure epoxy resin before (a & b) and after (c & d) single-mode microwave irradiation at 100w, 2.45 GHz for 3 mins.

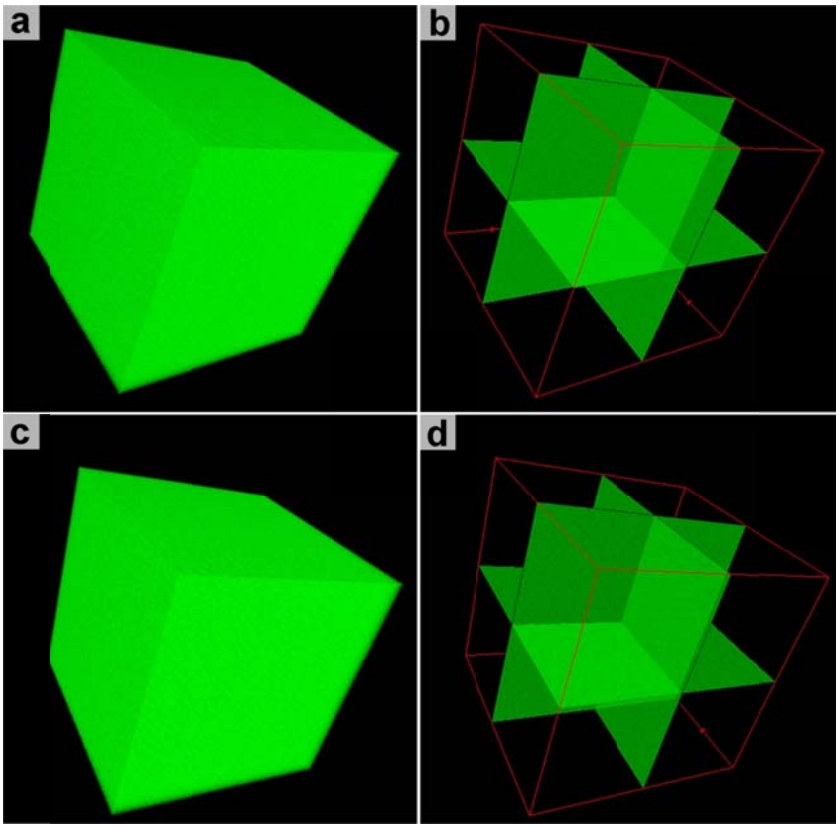

Fig. S4 3D X-ray computed tomography of cured pure epoxy resin before (a & b) and after (c & d) 3 mins' microwave irradiation at 100 w, 2.45 GHz. Figs. S4b and d are corresponding orthoslices for Figs. S4a and c, respectively. The side lengths of cubic are 100 μm.

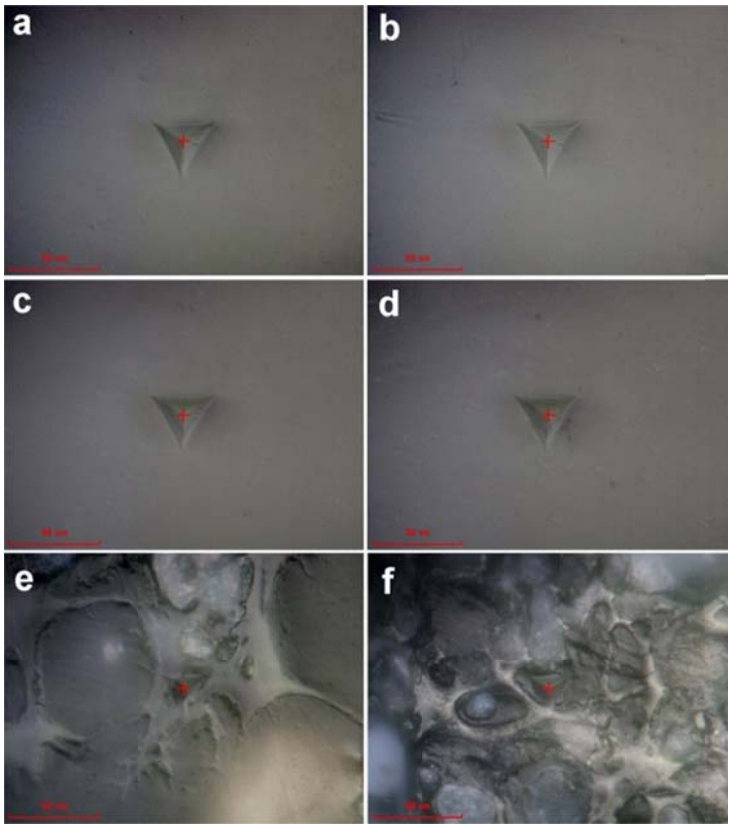

Fig. S5 The indentation sites of the pure epoxy resin before (a) and after 3 mins' dielectric heating (b), and indentation sites of the Fe_3O_4-ER nanocomposite adhesive before (c) / after 1(d), 2(e) and 3(f) min's dielectric heating.

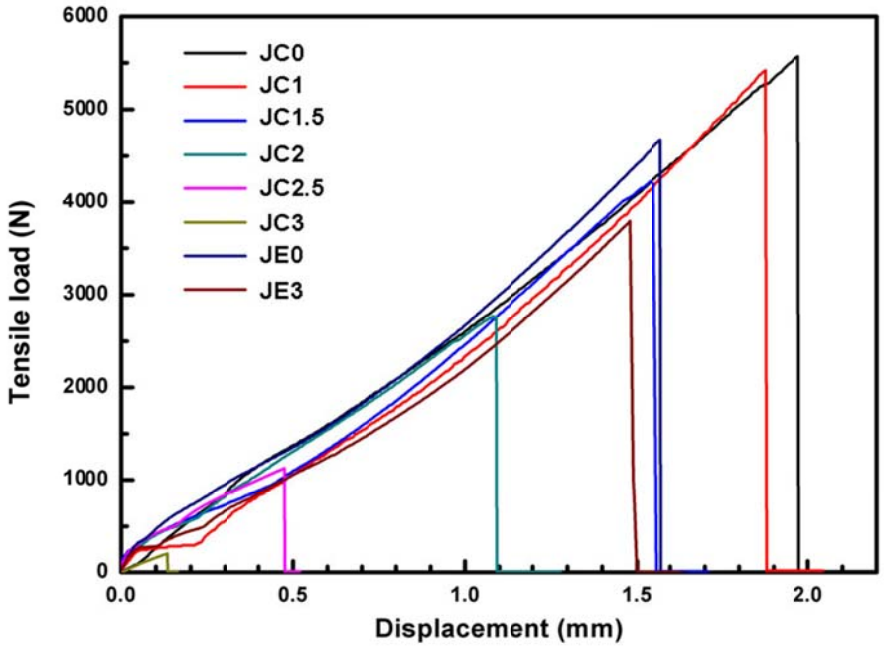

Fig. S6 The tensile shear load as a function of displacement for the adhesively-bonded single lap–shear (SLS) joints before and after dielectric heating. C_x = Joints bonded by Fe_3O_4-ER nanocomposite adhesive in x mins' microwave irradiation. E_x = Joints bonded pure epoxy resin in x mins' microwave irradiation.

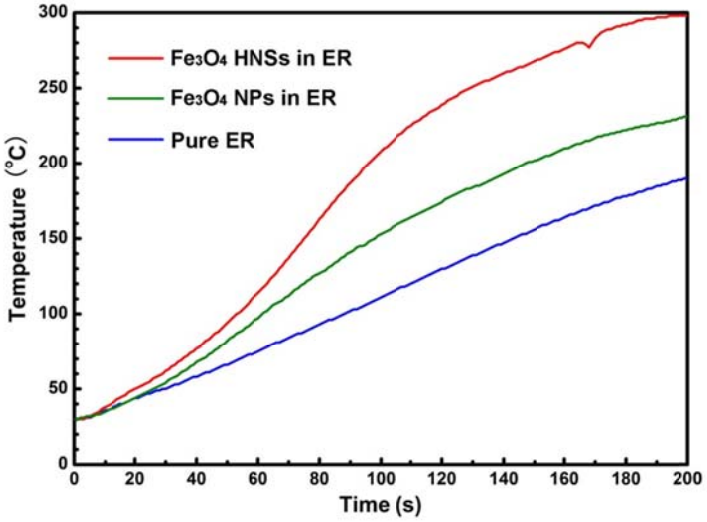

Fig. S7 Heating temperature as a function of time for the Fe_3O_4 HNSs in ER, Fe_3O_4 NPs in ER and pure epoxy resin under single-mode microwave irradiation at 100w, 2.45 GHz.

An experiment was supplemented to compare the dielectric heating performance of Fe_3O_4 nanoparticles (50-100 nm, Sigma-Aldrich) with hollow nanopsheres dispersed in epoxy resin in the same procedure. Fig. S7 shows the heating rate of Fe_3O_4 HNSs (1.0 wt%) and Fe_3O_4 NPs (1.0 wt%) in epoxy resin under single mode microwave irradiation at 100 w, 2.45 GHz, in the same procedure, indicating that temperature increasing speed of Fe_3O_4 NPs is quite lower than Fe_3O_4 HNSs.

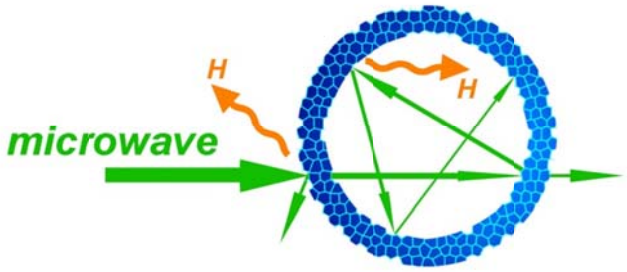

Fig. S8 Schematic illustrations of the microwave pathway in Fe_3O_4 HNSs. ("H" means thermal heating energy)

Previous works also reported the Fe_3O_4 with core-shell [8, 9-11] or hollow spherical [12-14] morphology could probably further enhance electromagnetic absorption performance [14]. A plausible mechanism was given in Fig. S8, when the microwave irradiation goes through the shell wall of hollow sphere, part of the microwave is absorbed by Fe_3O_4 due to magnetic loss, and most of this energy is converted into heating energy. In the meantime, part of the microwave is reflected by the outside shell and this part will probably meet another Fe_3O_4 HNSs, and the microwave partially goes through the shell and meets with the inner wall again. Followed by the same mechanism, the microwave irradiation is reflected by the inner wall several times, which can positively enhance the microwave absorption and heating efficiency [14].

Table S1 A summary of the hardness/modulus of adhesive and the failure load/strength of SLS joints by microwave irradiation over time

	The adhesive		SLS joints	
	Hardness	Modulus	Failure load	Strength
Neat epoxy resin				
t = 0 min	0.16 GPa	3.3 GPa	4670 N	7.2385 MPa
t = 3 min	0.16 GPa	3.4 GPa	3796 N	5.8838 MPa
Fe_3O_4-ER nanocomposite adhesive				
t = 0 min	0.20 GPa	3.6 GPa	5573 N	8.6382 MPa
t = 1 min	0.20 GPa	3.6 GPa	5420 N	8.4010 MPa
t = 2 min	0.17 GPa	3.0 GPa	2764 N	4.2842 MPa
t = 3 min	0.02 GPa	0.6 GPa	202 N	0.3126 MPa

References

1 N. Tripathy, R. Ahmad, H.-S. Jeong, Y.-B. Hahn, *Inorg. Chem.*, 2012, **51**, 1104–1110.

2 X. C. Li, V. T. John, G. H. He, J. B. He, L. Spinu, *J. Mater. Chem.*, 2012, **22**, 17476–17484.

3 D. P. Wang, H. C. Zeng, *Chem. Mater.*, 2009, **21**, 4811–4823.

4 M. Wang, Q. Zeng, B. Zhao, D. He, *J. Mater. Chem. A*, 2013, **1**, 11465–11472.

5 M. Hardiman, T. J. Vaughan, C. T. McCarthy, *Compos Part A*, 2015, **68**, 296–303.

6 P. Jojibabu, M. Jagannatham, P. Haridoss, G. D. J. Ram, A. P. Deshpande, S. R. Bakshi, *Composites Part A*, 2016, **82**, 53–64.

7 Y. Boutar, S. Naïmi, S. Mezlini, M. B. S. Ali, *Int. J. Adhes. Adhes.*, 2016, **67**, 38–43.

8 J. Liu, R. Che, H. Chen, F. Zhang, F. Xia, Q. Wu, M. Wang, *Small*, 2012, **8**, 1214–1221.

9 J. W. Liu, J. J. Xu, R. C. Che, H. J. Chen, M. M. Liu, Z. W. Liu, *Chem. Eur. J.*, 2013, **19**, 6746–6752.

10 J. J. Xu, J. W. Liu, R. C. Che, C. Y. Liang, M. S. Cao, Y. Li, Z. W Liu, *Nanoscale*, 2014, **6**, 5782–5790.

11 M. Yu, C. Y. Liang, M. M. Liu, X. L. Liu, K. P. Yuan, H. Cao, R. C. Che, *J. Mater. Chem. C*, 2014, **2**, 7275–7283.

12 H. L. Lv, G. B. Ji, W. Liu, H. Q. Zhang, Y. W. Du, *J. Mater. Chem. C*, 2015, **3**, 10232–10241.

13 Y. C. Du, W. W. Liu, R. Qiang, Y. Wang, X. J. Han, J. Ma, P. Xu, *ACS Appl. Mater. Interfaces*, 2014, **6**, 12997−13006.

14 R. Pang, X. J. Hu, S. Y. Zhou, C. H. Sun, J. Yan, X. M. Sun, S. Z. Xiao, P. Chen, *Chem. Commun.*, 2014, **50**, 12493–12496.